SIMULATING AND ESTIMATING SPALLING DEFECT DEPTH IN PASSIVE THERMOGRAPHY USING NEURAL NETWORK TECHNIQUES

RUDI HERIANSYAH and S. A. R. ABU-BAKAR

Faculty of Electrical Engineering, Universiti Teknologi Malaysia
81310 UTM Skudai, Johor, MALAYSIA
e-mail: rudihe@gmail.com, syed@fke.utm.my

Abstract: A method to simulate and to estimate the depth of the defects by means of passive thermography is proposed. Two artificial neural networks (ANN) paradigm: multilayer perceptrons (MLP) and radial basis functions (RBF) networks are employed for depth estimation. It has been found from simulation result that the following informative parameters: the maximum temperature within defective area ($T_{max\text{-}def}$), the average temperature on the right edge of the defect ($T_{avg\text{-}right}$), the average temperature on the top edge ($T_{avg\text{-}top}$), the average temperature within defect area ($T_{avg\text{-}def}$), and the average temperature within sound area ($T_{avg\text{-}so}$) have a relation with the spalling defect depth; hence they are proposed and used as input parameters for ANN training. ANN has been tested with trained and untrained data. The result shows a great potential of this paradigm for defect depth estimation in a passive thermography.

Keywords: infrared thermography, neural networks, MLP, RBF, spalling simulation, depth estimation

1 INTRODUCTION

Furnace linings may be single or multilayer form. Single layer usually suffices for furnaces operating at temperatures below 760^0C. Lining for modern high-temperature furnaces are almost always multilayer. The high temperature layer, which forms the interior surface of the refractory, referred to as 'hot-face', is backed by one or more layers of less-duty refractory and/or insulating materials, and finally the outer metal shell or 'skin' (cold-face) [Trinks et al, 2004].

At temperatures above 2000^0F (1367^0C), refractories become more and more porous, allowing the hot furnace gases to attack the chemistry of the refractory. In time, this attack reduces the surface strength of the refractories and causes their melting temperature to be lowered [Trinks et al, 2004].

Common defect which is occurred within refractory wall is the *spalling defect* which is the breaking or cracking of refractory brick in service, to such an extent those pieces are separated or fallen away, leaving new surfaces of the brick exposed [Griswold, 1946].

Since the crack or spalling defect within a refractory wall can cause heat losses to the external environment which can make the furnace: does not work at its optimum temperature, decreases efficiency, and increases operating cost. Therefore, the early sign of the defect existence should be known promptly. The potential techniques to assess the wall integrity are impact-echo method [Jaeger, 2000] and infrared thermography (IRT) [Maldague, 2001].

IRT uses the distribution of surface temperatures to assess the structure or behavior of what is under the surface [Maldague, 2001]. Thermal infrared camera is employed to record the temperature distribution which is called as *thermal image* or *thermogram* [Gaussorgues, 1994].

IRT has gained its popularity in the last few decades over other predictive maintenance techniques due to its many advantages. Being contactless, easy interpretation, large inspection coverage, and free from dangerous of radiation are among some of them. Above all, IRT has been successfully applied to solve many real world problems.

Based on how the thermogram is produced, IRT has two approaches: *active thermography*, where an external heat source is needed to stimulate the materials to be inspected, and *passive thermography*, where external heat source is not needed, in which the test materials or structures are naturally already at a different (often higher) temperature than ambient.

This paper discusses the method to simulate the spalling defect and to estimate its depth once occurred within a refractory furnace wall. The next section discusses the numerical method to simulate a spalling defect in a furnace wall. In Section 3, the informative parameters that reflect the existence of spalling defect are derived. Section 4 gives brief description on multilayer perceptrons (MLP) and radial basis functions (RBF) neural networks for

spalling defect depth estimation. Section 5 shows the experimental results for depth estimation. Lastly, Section 6 concludes and highlights the future works of this paper.

2 MODELING OF SPALLING DEFECT

In IRT, numerical modeling is a precious tool, especially since it can provide limits to the effectiveness of the thermal nondestructive testing (TNDT) technique and also the possibility of considering different defect geometries and determining their detectability without the expense of making and testing the corresponding specimens [James et al, 1989].

Other purpose of numerical modeling in IRT is to simulate the real situation in order to obtain the simulated thermogram from that simulation [Conner, 1998]. This thermogram can be used to test the developed algorithms (mainly related to image processing) in case of the unavailability of the thermogram from the real object, for instance due to the difficulties to obtain such thermal data.

From modeling tools perspective, there are two common methods for numerical modeling in IRT that are finite difference method (FDM) [Özişik, 1994; Croft and Lilley, 1977] and finite element method (FEM) [Segerlind, 1984; Rao, 1989]. FDM is simple and easy to implement but it suffers when handling irregular geometry or anisotropic materials. FEM although is quite complex but it can work elegantly on deformed shape and non-homogeneous materials [ElShayeb and Beng, 2000], can improve accuracy and efficiency [Huebner et al, 1995].

In IRT, currently the application of FEM is widely used. Although in the early years FDM was usually employed for heat behavior study [Saintey and Almond, 1997], but in the last few years, the trend shows that FEM is common alternative used by researchers [Krishnapillai et al, 2006]. This paper takes the advantage of FEM for modeling the spalling defect.

Consider a typical four layers furnace wall in Figure 1(a). The thermal properties of these layers are given in Table 1, where k is the thermal conductivy and ρ is the bulk density.

The spalling defect is simulated as a *void* occurred within refractory firebrick wall or the hot-face wall. The *defect depth* is defined as its depth from the outer wall (cold-face steel casing wall) or measured as the difference between the total lengths of the layered walls with the *defect thickness*. Figure 1(b) shows a portion of simulated wall with length of 80cm and width of 40cm. In this figure, the defect is

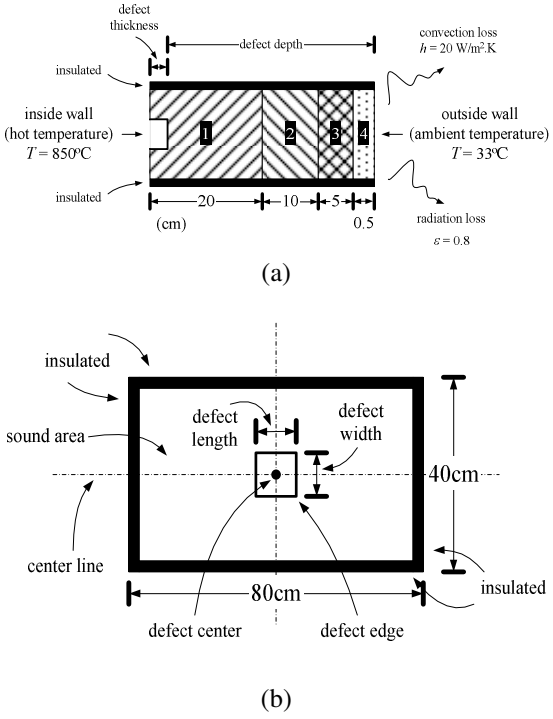

Figure 1: Typical four layers furnace wall: (a) side-view, and (b) front view

Table 1: Thermal properties

Materials		k (W/m.K)	ρ (kg/m^3)
No.	Name		
1	Firebrick	1.436	2300
2	Insulation	0.225	1200
3	Fiber block	0.116	430
4	AISI 316 Steel	16.3	8000

located in the center of the wall model. Some terms introduced in this paper are also shown in the figure.

For passive thermography case, it is assumed that the temperature has been at its steady-state condition, in our case, the hot-face wall temperature assumed constant at 850^0C, with ambient temperature to be at 33^0C. Adiabatic boundary conditions are applied to the four sides of the wall. Losses due to convective (with convection coefficient, h = 20 W/m^2.K) and radiative (with emissivity, ε = 0.8) heat transfer occur from the outer surface (cold-face) wall.

To save the processing time, coarse elements were used in meshing process. Figure 2 shows the meshing result with 4cm element size of the modeled wall. Figure 3(a) shows the temperature distribution on the outer steel casing wall and Figure 3(b) shows the temperature distribution over the defect area along the center line of the wall. From this figures it is clear that due to the existence of the subsurface defect, an elevated temperatures are

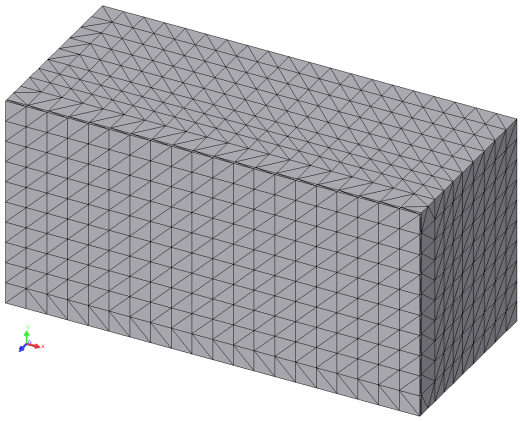

Figure 2: Model after meshing operation

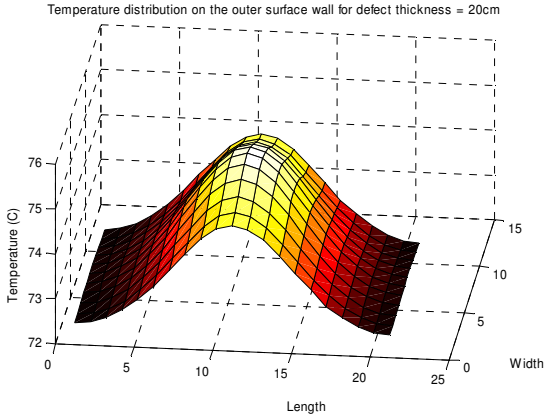

(a)

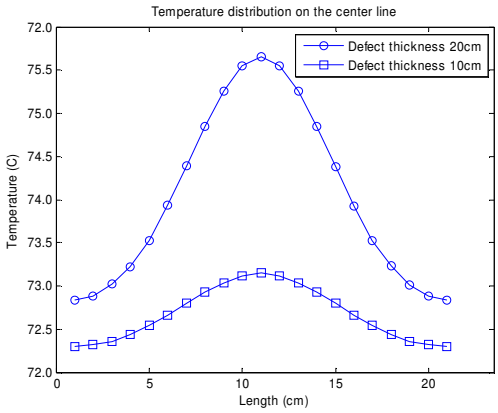

(b)

Figure 3: (a) Temperature distribution on the outer surface wall, (b) temperature distribution over the defect area along the center line of the wall for defect thickness 20cm and 10cm with defect size 15cm×15cm

observed over the defect area as reflected on the outer surface wall. From the figure, the maximum temperature occurred on the center of the defect and gradually decreases near the defect edges.

3 INFORMATIVE PARAMETERS

Figure 3(b) clearly showed that temperature distribution on the outer wall surface has a relation with defect depth (thickness). It was also confirmed by the previous research [Heriansyah and Abu-Bakar, 2007] that there is strong interdependence between the defect depth and the *maximum temperature over the defect area* ($T_{max\text{-}def}$) as depicted in a thermal image of furnace wall.

If the spalling defect shape is uniform then due to the symmetry property of the finite element model, this maximum value will always be the peak value or at the defect center as shown in Figure 3. Figure 4 shows relation of defect depth with maximum temperature value within defect area. It is obvious that the deeper thickness of the defect or the shallower defect depth from the outer surface will increase the temperature value at that surface.

From Figure 3, it shows that from the peak, the temperature gradually decrease to the model edge. Therefore, at the defect edge (left, right, top, and bottom) the temperature is less small than at the peak. Again, due to the symmetry property, for a uniform spalling at the left and right, and the top and the bottom of the defect edge will always has equal temperature value. Figure 4 shows the relation of defect depth with temperature at the right and top edge of the defect. In this paper, the *average temperature of the right edge* ($T_{avg\text{-}right}$) and the *average temperature of the top edge* ($T_{avg\text{-}top}$) are used as the informative parameters.

As the temperature increases due to the defect depth, the *average temperature over defect area* ($T_{avg\text{-}def}$) reflected at the outer wall will also increase as shown in Figure 4. The same situation is also observed for the *average temperature on the sound* (non-defective) area ($T_{avg\text{-}so}$) as shown in Figure 5. These figures also tell us that relation of defect depth with these informative parameters ($T_{max\text{-}def}$, $T_{avg\text{-}right}$, $T_{avg\text{-}top}$, $T_{avg\text{-}def}$, $T_{avg\text{-}so}$) tend to have linear property. Note that all these parameters derived from a fix defect size and the defect is situated at the center of the wall model (Figure 1(b)).

Figure 6 shows the wall model with 15cm×15cm defect size and 20cm of defect thickness, and the defect is located at the *top-right corner* of the wall model. Figure 7 shows the temperature distribution at the outer surface wall and at the center line. It is clear that due to nonsymmetrical position of the spalling defect, the temperature distribution reflected at the outer surface wall is nonsymmetry as well. Another fact also confirmed that elevated temperatures occurred over the defect area and defect depth has relation with temperature values.

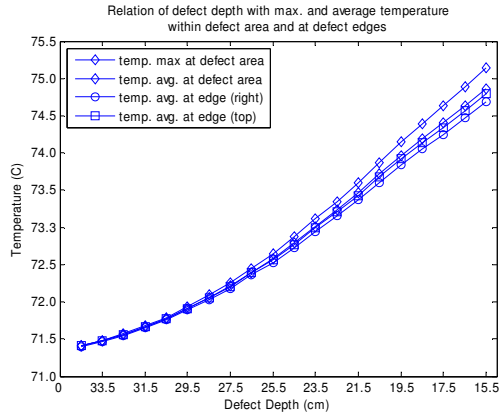

Figure 4: Relation of defect depth with maximum and average temperature within defect area and at right and top edges

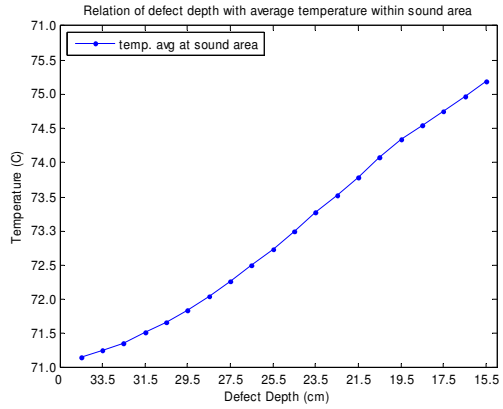

Figure 5: Relation of defect depth with average temperature within sound area

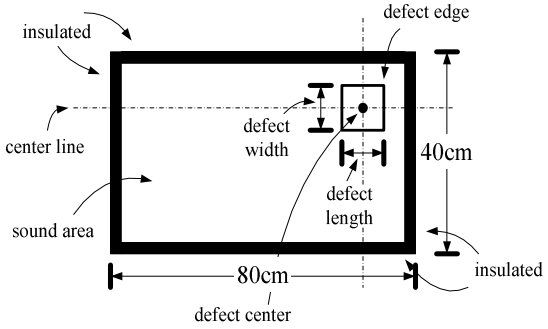

Figure 6: Front view of spalling defect located at the top-right corner of the wall model

The temperature increases as the defect depth decreases (or defect thickness increases).

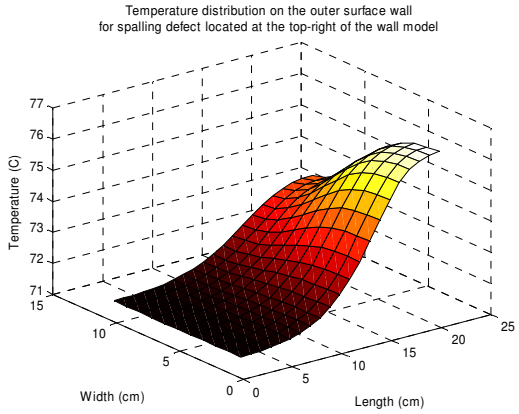

(a)

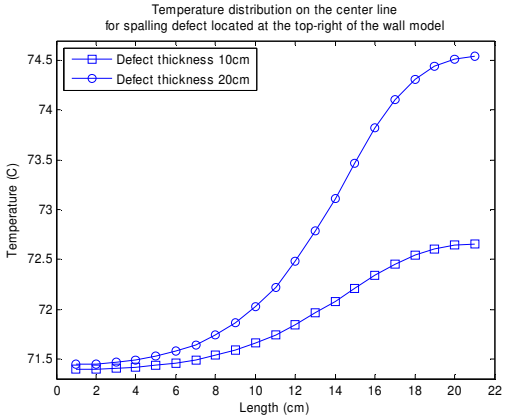

(b)

Figure 7: (a) Temperature distribution on the outer surface wall for the spalling defect located at the top-right corner of the wall model, (b) temperature distribution over the defect area along the center line of the wall for defect thickness 20cm and 10cm with defect size 15cm×15cm

4 MLP AND RBF NETWORK BASED DEPTH ESTIMATOR

Artificial neural network (ANN) is a simple abstraction of biological neurons. Networks of these artificial neurons do not have a fraction of the power of the human brain, but they can be trained to perform useful functions [Hagan et al, 1996].

In recent years many researchers have used ANN to solve complex nonlinear real world problems. ANNs are potentially powerful, robust and adaptive tools for detecting and classifying targets under changing signature or environmental conditions [Darabi and Maldague, 2002].

These capabilities have motivated some researchers to employ ANN to solve their thermography problems. Saintey and Almond (1997), used finite difference modeling to generate input training data for neural network interpreter to determine defect size and depth. Darabi and Maldague (2002), did a similar approach in which they used three dimensional heat transfer models to generate synthetic data to train neural network depth estimator by means of active thermography. All existing depth estimation based on ANN [Saintey and Almond, 1997; Darabi and Maldague, 2002; Maldague et al, 1998; Manduchi et al, 1997; Vallerand and Maldague, 2000; D'Orazio et al, 2005] were designed for active thermography application. This paper uses numerical method to simulate the spalling defect behavior in term of temperature distribution and to employ this simulated result as the input parameters to train ANN for defect depth estimation in a passive thermography scheme.

In this paper, a *multilayer perceptrons* (MLP) and *radial basis function* (RBF) neural networks [Haykin, 1994] were trained to have the capability in the estimation of defect depth which may occur within the furnace refractory. MLP was selected as depth estimator since it is a common ANN paradigm used for various applications with satisfactory results [Jain and Fanelli, 2000]. While, RBF was selected as the comparator, actually is not really 'to compare' but as an alternative way when using ANN approach for this specific application.

As already shown in the previous section, the maximum temperature over the defect area ($T_{max\text{-}def}$), the average temperature at the right edge ($T_{avg\text{-}right}$), the average temperature at the top edge ($T_{avg\text{-}top}$), the average temperature within defect area ($T_{avg\text{-}def}$), and the average temperature within the sound area ($T_{avg\text{-}so}$) are indeed related to the spalling defect depth. Therefore, these five parameters are employed in the ANN training for spalling depth estimation. These parameters are extracted from the numerical modeling as discussed in the previous section.

For the training purpose, the following defect depths are used: 34.5, 33.5, 32.5, 31.5, 30.5, 29.5, 28.5, 27.5, 26.5, 25.5, 24.5, 23.5, 22.5, 21.5, 20.5, 19.5, 18.5, 17.5, 16.5, and 15.5 cm. Again, note that defect depth in our case is measured from the outer face (steel) wall (refer to Figure 1(a)).

5 RESULTS AND DISCUSSION

The input data for training are $T_{max\text{-}def}$, $T_{avg\text{-}right}$, $T_{avg\text{-}top}$, $T_{avg\text{-}def}$ and $T_{avg\text{-}so}$ and the corresponding values of defect depth were used as the outputs. One hidden layer with eight nodes of MLP was found to be effective for this purpose. The transfer functions are *tangent-sigmoid* and *linear* for the first and second layer respectively. The *scaled conjugate gradient* (SCG) algorithm (with λ = 5.0e-7) was used to train the MLP. During the training session, *mean squared error* (MSE) and *sum-squared error* (SSE) functions were employed to check the MLP and RBF network performance respectively. *Gaussian* and *linear* threshold functions were used for RBF architecture with 18 *centers* and *spread* value of 1.0 [Demuth and Beale, 2001].

Figure 8 shows the defect depth estimation results by both networks for the trained data as compared to the actual depth. Errors for depth estimation in both cases were found to be zero, or 100% correct estimation.

Figure 9 shows the depth estimation for untrained data (of depth 35, 34, 33, 32, 31, 30, 29, 28, 27, 26, 25, 24, 23, 22, 21, 20, 19, 18, 17, and 16cm respectively from the outer surface wall). Depth estimation error for this untrained data is shown in Table 2 for MLP and in Table 3 for RBF network result.

From Table 2, for the case of *center spalling* defect (Center), there is no depth estimation error for all defects except for defect with depth 35cm, the error is around 2.86%. MLP can estimate correctly without error for 19 other depths (34 to 16cm). For the case of *top-right corner spalling* defect (Corner), all errors are no more than 12.50% or even for the worst case, the accuracy is still around 87.50%. In which, 15 depths (35 to 21cm) have error less than 5% (95% accuracy), and 5 depths (20 to 16cm) have error less than 13% (87% accuracy). Thus, the average error for center spalling is 0.14% (99.86% accuracy), and the average error for top-right corner spalling is 5.54% (94.46% accuracy).

From Table 3, for the case of *center spalling* defect, RBF can estimate correctly for all defect depths without error. For *top-right corner spalling*, the worst estimation is for 16cm depth, the error is greater than 60%. The next worst are in estimating 17cm and 18cm depths, with errors greater than 50% and 30% respectively. For the other depths, the estimation error is all under 30% (70% accuracy). Hence, the average error for center defect is 0% (100% accuracy), and 13.27% (86.73% accuracy) for the case of top-right corner defect.

6 CONCLUSIONS

It has been shown from the result in the previous section that the depth estimation by using MLP and RBF neural networks paradigm both for trained and

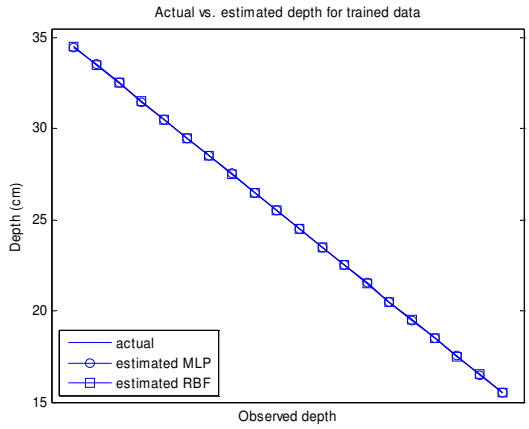

Figure 8: Estimated depth for trained data

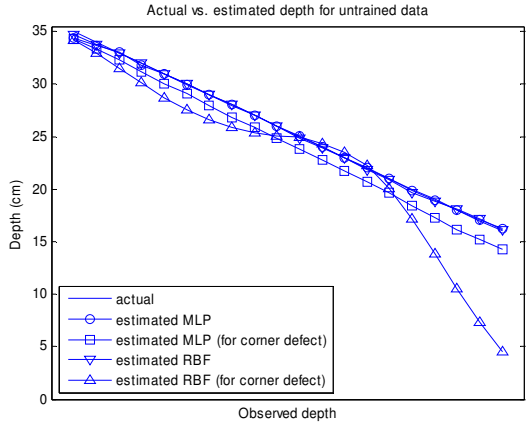

Figure 9: Estimated depth for untrained data

untrained data is quite satisfactory. There is no estimation error for both networks for trained data. The average error for untrained data for MLP is less than 1% for the case of center defect, and less than 6% for the case of top-right corner defect. The average error for RBF is 0% for the case of center defect, and less than 14% for the case of top-right corner defect.

It is shown that the average error for RBF is quite greater than MLP for the case of top-right corner spalling, but it can estimate correctly for all depths for the case of center spalling type defect. Therefore as the rule of thumb, we can say generally that in this specific application MLP is better than RBF for both cases. Even with the lack of training data and quite different testing data, MLP still can give proper estimation results.

The results also showed that the informative parameters ($T_{max\text{-}def}$, $T_{avg\text{-}right}$, $T_{avg\text{-}top}$, $T_{avg\text{-}def}$ and $T_{avg\text{-}so}$) proposed in this paper are suitable for depth estimation in passive thermography. As already shown in previous section, these informative parameters have a relationship with spalling defect depth. Although these informative parameters will give a slightly different values for different spalling defect location in the model (as shown in Figure 7), but still with these five parameters, ANN give a satisfactorily results for trained and untrained data for both networks.

Table 2: Depth estimation error for untrained data of MLP networks

Actual Depth	Estimated Depth		Error (%)	
	Center	Corner	Center	Corner
35	34	34	2.86	2.86
34	34	33	0	2.94
33	33	32	0	3.03
32	32	31	0	3.13
31	31	30	0	3.23
30	30	29	0	3.33
29	29	28	0	3.45
28	28	27	0	3.57
27	27	26	0	3.70
26	26	25	0	3.85
25	25	24	0	4.00
24	24	23	0	4.17
23	23	22	0	4.35
22	22	21	0	4.55
21	21	20	0	4.76
20	20	18	0	10.00
19	19	17	0	10.53
18	18	16	0	11.11
17	17	15	0	11.76
16	16	14	0	12.50

Table 3: Depth estimation error for untrained data of RBF networks

Actual Depth	Estimated Depth		Error (%)	
	Center	Corner	Center	Corner
35	35	34	0	2.86
34	34	33	0	2.94
33	33	31	0	6.06
32	32	30	0	6.25
31	31	29	0	6.45
30	30	28	0	6.67
29	29	27	0	6.90
28	28	26	0	7.14
27	27	25	0	7.41
26	26	25	0	3.85
25	25	25	0	0.00
24	24	24	0	0.00
23	23	24	0	-4.35
22	22	22	0	0.00
21	21	20	0	4.76
20	20	17	0	15.00
19	19	14	0	26.32
18	18	11	0	38.89
17	17	7	0	58.82
16	16	5	0	68.75

This paper has demonstrated on how to employ ANN paradigm for depth estimation in a passive thermography. Two NN paradigms: MLP and RBF networks have been employed and the results are promised. For future works, other informative parameters can be explored. In addition, to preserve the spalling defect location property, ANN can be trained with more input data to achieve a better generalization.

ACKNOWLEDGMENT

This work was supported by the Ministry of Science, Technology, and Innovations (MOSTI), Malaysia government through research grant, vote no. 74271. The authors would like to express their gratitude to the government of Malaysia and the Universiti Teknologi Malaysia for providing a good research atmosphere and any high-end facilities, hence make this work run smoothly.

REFERENCES

Conner, D. J. 1998, *Thermographic Defect Detection and Classification from Noisy Infra-red Image Sequences*. The Catholic University of America: Ph.D Thesis.

Croft, D. R. and Lilley, D. G. 1977, *Heat Transfer Calcultions using Finite Difference Equations.* Applied Science Publishers, Ltd.

D'Orazio, T., Guaragnella, C., Leo, M., and Spagnolo, P. 2005, "Defect Detection in Aircraft Composites by using a Neural Approach in the Analysis of Thermographic Images", *NDT&E International*, No. 38, pp. 665-673.

Darabi, A. and Maldague, X. 2002, "Neural Network based Defect Detection and Depth Estimation in TNDE", *NDT&E International*, No. 35, pp. 165-175.

Demuth, H. and Beale, M. 2001, *Neural Network Toolbox for use with MATLAB*, The MathWorks, Inc.

ElShayeb, M. and Beng, Y. K. 2000, *Application of Finite Difference and Finite Element Methods for Thermal Problems.* Sabah, Malaysia: Universiti Malaysia Sabah.

Gaussorgues, G. 1994, *Infrared Thermography*, Cambridge: Chapman & Hall.

Griswold, J. 1946, *Fuels, Combustion, and Furnaces*, McGraw-Hill Book Company, Inc.

Hagan, M. T., Demuth, H. B., and Beale, M. 1996, *Neural Network Design*, Boston, PWS Publishing Company.

Haykin, S. 1994, *Neural Networks: A Comprehensive Foundations*, New York, Macmillan College Publishing Company Inc.

Heriansyah, R. and Abu-Bakar, S. A. R. 2007, "Modeling of Defects within High Temperature Wall by Means of Infrared Thermography", Proceedings of the International Conference on Risk Technology & Management, pp. 298-302.

Huebner, K. H., Thornton, E. A., and Byrom, T. G. 1995, *The Finite Element Method for Engineers*. 3rd ed. Canada: John Wiley & Sons, Inc.

Jaeger, B. J. 2000, "Refractory Wall Thickness Measurements in High Temperature Environments and in Thermal and Material Property Gradients using the Impact-echo Method", Cornell University: PhD Dissertation.

Jain, L. and Fanelli, A. M. 2000, *Recent Advances in Artificial Neural Networks: Design and Applications*, Boca Raton, CRC Press LLC.

James, P. H., Welch, C. S., and Winfree, W. P. 1989, "A Numerical Grid Generation Scheme for Thermal Simulation in Laminated Structures", in Thompson, D. O. and Chimneti, D. E., eds., *Review in Progress in Quantitative Nondestructive Evaluation*, No. 8A, pp. 801-809.

Krishnapillai, M., Jones, R., Marshall, I. H., Bannister, M., and Rajic, N. 2006, "NDTE using Pulse Thermography: Numerical Modeling of Composite Subsurface Defects". *Composite Structures.* 75: 241-249.

Maldague, X. P. V. 2001, *Theory and Practice of Infrared Technology for Nondestructive Testing*. John Wiley & Sons, Inc.

Maldague, X., Largouët, Y., and Couturier, J. P. 1998, "A Study of Defect Depth using Neural Networks in Pulsed Phase Thermography: Modelling, Noise, Experiments", *Rev. Gén. Therm.*, No. 37, pp. 704-717.

Manduchi, G., Marinetti, S., Bison, P., and Grinzato, E. 1997, "Application of Neural Network Computing to Thermal Non-destructive Evaluation", *Neural Computing & Applications*, No. 6, pp. 148-157.

Özişik, M. N. 1994, *Finite Difference Methods in Heat Transfer*. CRC Press, Inc.

Rao, S. S. 1989, *The Finite Element Method in Engineering*. 2nd ed. Oxford, England: Pergamon Press plc.

Saintey, M. B. and Almond, D. P. 1997, "An Artificial Neural Network Interpreter for Transient Thermography Image Data", *NDT&E International*, No. 5, pp. 291-295.

Segerlind, L. J. 1984, *Applied Finite Element Analysis.* 2nd ed. John Wiley & Sons, Inc.

Trinks, W., Mawhinney, M. H., Shannon, R. A., Reed, R. J., and Garvey, J. R. 2004, *Industrial Furnaces*, ed. **6**, John Wiley & Sons, Inc.

Vallerand, S. and Maldague, X. 2000, "Defect Characterization in Pulsed Thermography: a Statistical Method Compared with Kohonen and Perceptron Neural Networks", *NDT&E International,* No. 33, pp. 307-315.

AUTHOR BIOGRAPHIES

RUDI HERIANSYAH was born in Palembang, Indonesia. He received the B.Eng (magna cum laude) and M.Eng degrees both in electrical engineering from Universitas Muhammadiyah Palembang, Palembang, Indonesia and Universiti Teknologi Malaysia, Johor, Malaysia in 1999 and 2004 respectively. He is currently pursuing Ph.D degree in the Faculty of Electrical Engineering, Universiti Teknologi Malaysia, Johor, Malaysia, working on the area of image processing and infrared thermography. He was an IT technical support and a professional database programmer before tuning himself to the academic field and doing research in the image processing area for the last seven years. He was an invited visiting researcher at Kochi University of Technology, Kochi, Japan in May 2006.

S. A. R. ABU-BAKAR was born in Johor, Malaysia. He received the B.Eng (with distinction), M.Eng, and Ph.D degrees all in electrical engineering from Clarkson University, New York, USA; Georgia Institute of Technology, Atlanta, USA; and Bradford University, Bradford, UK in 1990, 1992, and 1997 respectively. He is currently an Associate Professor at the Department of Microelectronics and Computer Engineering, Faculty of Electrical Engineering, Universiti Teknologi Malaysia, Johor, Malaysia. He heads the Digital Lab and Computer Vision, Video, and Image Processing Research Lab (CVVIP). His current research interests include image processing, moving object detection, and stereo vision.